J|A|C|S
ARTICLES
Published on Web 09/24/2002

Single-Crystal Mesostructured Semiconductors with Cubic *Ia*$\bar{3}$*d* Symmetry and Ion-Exchange Properties

Pantelis N. Trikalitis,[†] Krishnaswamy K. Rangan,[†] Thomas Bakas,[‡] and Mercouri G. Kanatzidis*[,†]

Contribution from the Department of Chemistry, Michigan State University, East Lansing, Michigan 48824, and Department of Physics, University of Ioannina, Ioannina, 45110 Greece

Received March 29, 2002

Abstract: If the full scientific and technological potential of mesostructured materials is to be achieved, systems with continuous domains in the form of single crystals or films must be prepared. Here we report a reliable and facile system for making large single-crystal particles of chalcogenido mesostructured materials with a highly organized cubic structure, accessible pore structure, and semiconducting properties. Building blocks with square planar bonding topology, Pt^{2+} and $[Sn_2Se_6]^{4-}$, in combination with long-chain pyridinium surfactants (C_nPyBr, $n = 18, 20$) favor faceted single-crystal particles with the highest possible space group symmetry *Ia*$\bar{3}$*d*. This is an important step toward developing large single-domain crystalline mesostructured semiconductors and usable natural self-assembled antidot array systems. The tendency toward cubic symmetry is so strong that the materials assemble readily under experimental conditions that can tolerate considerable variation and form micrometer-sized rhombic dodecahedral cubosome particles. The *c*-C_nPyPtSnSe materials are the first to exhibit reversible ion-exchange properties. The surfactant molecules can be ion-exchanged reversibly and without loss of the cubic structure and particle morphology. The cubosomes possess a three-dimensional open Pt−Sn−Se framework with a low-energy band gap of ∼1.7 eV.

Introduction

Materials with ordered and controllable structural features at the mesoscale (20−200 Å) are of exceptionally broad interest because of anticipated high technological impact in catalysis,[1,2] separation science,[3] inclusion chemistry,[4] sensors,[5] and optical[6] and electronic materials,[7] among others. Since the first report of mesoporous silicates[8] almost a decade ago, numerous mesoporous and mesostructured silica-based materials,[1,9] metal oxides,[10] and pure metals[5,11] have been reported and significant advances were made in controlling the overall structure. Although, these materials are believed to be amorphous on the atomic scale, they can possess periodic long-range pore order in two- or three-dimensions. Among these, the hexagonal MCM-41 type is the most well studied and frequently reported; however, the cubic three-dimensional (3D) pore structures are increasingly recognized to be much more interesting and desirable in terms of their potential.[12,13] For example, 3D mesoporous materials begin to find unique uses including molds for the creation of mesostructured metals,[14] metal oxides,[15] and carbon (nanocasting).[16]

* To whom correspondence should be addressed. E-mail: kanatzid@cem.msu.edu.
[†] Michigan State University.
[‡] University of Ioannina.

(1) Corma, A. *Chem. Rev.* **1997**, *97*, 2373−2419.
(2) Climent, M. J.; Corma, A.; Iborra, S.; Miquel, S.; Primo, J.; Rey, F. *J. Catal.* **1999**, *183*, 76−82.
(3) (a) Kisler, J. M.; Dahler, A.; Stevens, G. W.; O'Connor, A. J. *Microporous Mesoporous Mater.* **2001**, *44*, 769−774. (b) Feng, X.; Fryxell, G. E.; Wang, L. Q.; Kim, A. Y.; Liu, J.; Kemner, K. M. *Science* **1997**, *276*, 923−926. (c) Han, Y. J.; Stucky, G. D.; Butler, A. *J. Am. Chem. Soc.* **1999**, *121*, 9897−9898. (d) Brown, J.; Mercier, L.; Pinnavaia, T. J. *Chem. Commun.* **1999**, 69−70.
(4) (a) Moller, K.; Bein, T. *Chem. Mater.* **1998**, *10*, 2950−2963. (b) Yiu, H. H. P.; Wright, P. A.; Botting, N. P. *Microporous Mesoporous Mater.* **2001**, *44*−*45*, 763−768.
(5) Attard, G. S.; Bartlett, P. N.; Coleman, N. R. B.; Elliott, J. M.; Owen, J. R.; Wang, J. H. *Science* **1997**, *278*, 838−840.
(6) (a) Yang, P. D.; Wirnsberger, G.; Huang, H. C.; Cordero, S. R.; McGehee, M. D.; Scott, B.; Deng, T.; Whitesides, G. M.; Chmelka, B. F.; Buratto, S. K.; Stucky, G. D. *Science* **2000**, *287*, 465−467. (b) Miller, L. W.; Tejedor, M. I.; Nelson, B. P.; Anderson, M. A. *J. Phys. Chem. B* **1999**, *103*, 8490−8492. (c) Dag, O.; Ozin, G. A.; Yang, H.; Reber, C.; Bussiere, G. *Adv. Mater.* **1999**, *11*, 474.
(7) (a) Nguyen, T. Q.; Wu, J. J.; Doan, V.; Schwartz, B. J.; Tolbert, S. H. *Science* **2000**, *288*, 652−656. (b) Baskaran, S.; Liu, J.; Domansky, K.; Kohler, N.; Li, X. H.; Coyle, C.; Fryxell, G. E.; Thevuthasan, S.; Williford, R. E. *Adv. Mater.* **2000**, *12*, 291−294.
(8) Kresge, C. T.; Leonowicz, M. E.; Roth, W. J.; Vartuli, J. C.; Beck, J. S. *Nature* **1992**, *359*, 710−712.
(9) (a) Oye, G.; Sjoblom, J.; Stocker, M. *Adv. Colloid Interface Sci.* **2001**, *89*, 439−466. (b) Stein, A.; Melde, B. J.; Schroden, R. C. *Adv. Mater.* **2000**, *12*, 1403−1419. (c) Ying, J. Y.; Mehnert, C. P.; Wong, M. S. *Angew. Chem., Int. Ed.* **1999**, *38*, 56−77.
(10) (a) Schuth, F. *Chem. Mater.* **2001**, *13*, 3184−3195. (b) Ma, Y.; Tong, W.; Zhou, H.; Suib, S. L. *Microporous Mesoporous Mater.* **2000**, *37*, 243−252. (c) Yang, P. D.; Zhao, D. Y.; Margolese, D. I.; Chmelka, B. F.; Stucky, G. D. *Nature* **1998**, *396*, 152−155. (d) Yang, P. D.; Deng, T.; Zhao, D. Y.; Feng, P. Y.; Pine, D.; Chmelka, B. F.; Whitesides, G. M.; Stucky, G. D. *Science* **1998**, *282*, 2244−2246. (e) Antonelli, D. M.; Ying, J. Y. *Angew. Chem., Int. Ed. Engl.* **1996**, *35*, 426−430.
(11) Attard, G. S.; Goltner, C. G.; Corker, J. M.; Henke, S.; Templer, R. H. *Angew. Chem., Int. Ed. Engl.* **1997**, *36*, 1315−1317.
(12) (a) Sakamoto, Y. H.; Kaneda, M.; Terasaki, O.; Zhao, D. Y.; Kim, J. M.; Stucky, G.; Shim, H. J.; Ryoo, R. *Nature* **2000**, *408*, 449−453. (b) Pena, M. L.; Kan, Q.; Corma, A.; Rey, F. *Microporous Mesoporous Mater.* **2001**, *44*, 9−16. (c) Xu, J.; Luan, Z. H.; He, H. Y.; Zhou, W. Z.; Kevan, L. *Chem. Mater.* **1998**, *10*, 3690−3698. (d) Morey, M. S.; Davidson, A.; Stucky, G. D. *J. Porous Mater.* **1998**, *5*, 195−204.
(13) Sayari, A. *J. Am. Chem. Soc.* **2000**, *122*, 6504−6505.

Chart 1

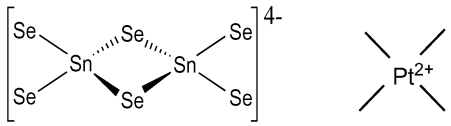

To date the vast majority of reports have focused on silicas, silicates, and other oxidic materials. Still in its infancy, the field of non-oxidic mesostructured materials, such metal chalcogenides, offers new capability in catalysis, separations, quantum electronics,[17] photonics,[18] and nonlinear optics.[19] Three-dimensional periodically arranged pores in a semiconducting solid could modify the optoelectronic properties in way that has no precedent in bulk semiconductor analogues. In this context we could create quantum "antidot" type superstructures, which are the negative image of quantum dot arrays.[20,21] Alternatively, these pores may serve as host space for adsorption or chemical reactions utilizing the properties of the framework and enabling electronically or optically driven processes not possible with the silicates. Because hexagonal systems with their unidirectional pore organization could frustrate guest diffusion, cubic 3D mesostructured semiconductors are much more attractive. Systems that favors cubic symmetry remain elusive,[22] despite recent reports on hexagonal mesostructured non-oxidic solids based on topological tetrahedral clusters.[23,24]

We report here that Pt^{2+} and $[Sn_2Se_6]^{4-}$, Chart 1, readily assemble into highly ordered *cubic* mesostructures with a MCM-48-type symmetry. Moreover, these are the first non-oxidic mesostructures to exhibit reversible ion-exchange properties. Both building blocks present local *square planar* connectivity preference and as such define the only currently available system that leads reliably to cubic chalcogenido mesostructures. The tendency toward cubic symmetry is so strong in this case that the materials assemble readily into single cubic particles of micrometer size.

Table 1. Elemental Analyses, Colors, and Energy Band Gaps for the Cubic Mesostructured Platinum Tin Selenides

sample	% C, H, N	TGA wt loss (%)	Se:Sn[a]	Pt:Sn[a]	color	band gap (eV)
c-C_{18}PyPtSnSe	32.92, 5.16, 1.93 35.15, 5.35, 1.78[b]	34.3	2.89	0.96	dark brown	1.64
c-C_{20}PyPtSnSe	36.14, 5.61, 1.78 36.90, 5.66, 1.72[b]	43.4	2.87	1.03	dark brown	1.75

[a] Based on energy-dispersive spectroscopy (EDS) results. Quantitative microprobe analyses (EDS) were performed on a JEOL JSM-6400V scanning electron microscope (SEM) equipped with a Noran EDS system. Data acquisition was performed several times in different areas of the samples using an accelerating voltage of 20 kV and 100 s accumulation time. Quoted values were obtained from an average of four measurements. [b] Expected C, H, and N values based on $(C_nPy)_2PtSn_2Se_6$.

Experimental Section

Starting Materials. $K_4Sn_2Se_6$ was prepared according to ref 25. K_2PtCl_4 was purchased from Strem Chemical Inc. The surfactants C_nPyBr ($n = 12, 18, 20$) were synthesized by reacting the corresponding alkyl bromide with excess pyridine in ethanol under reflux conditions. Pure compounds were obtained in 90% yield after single recrystallization from $CHCl_3$−ethyl acetate.

Synthesis of Cubic Platinum Tin Selenides *c*-C_nPyPtSnSe. In a typical preparation, 4 g of surfactant C_nPyBr ($n = 18, 20$) and 0.867 g (1 mmol) of $K_4Sn_2Se_6$ were dissolved in formamide (FM) at 80 °C forming a clear orange-red solution. In a separate flask a solution of 0.415 g (1 mmol) of K_2PtCl_4 in 10 mL of FM was heated at 80 °C to form a red-orange solution, and this was added to the surfactant/$[Sn_2Se_6]^{4-}$ solution over a period of 2 min using a pipet. A dark brown-red solid was formed within a few seconds, and the mixture was aged overnight at 80 °C under stirring. The product was isolated by filtration, washed with copious amount of warm (80 °C) FM and H_2O, and dried under vacuum. Yield: >80% based on $K_4Sn_2Se_6$. Substantial variation of the surfactant amount (±50%) and temperature (range 40−80 °C) did not materially affect product yield or quality. The syntheses and characterization experiments were repeated many times to ensure reproducibility. In all cases a single product with reproducible results was obtained. Syntheses were performed in a glovebox under nitrogen.

Ion Exchange. A 1.5 g amount of pristine *c*-C_{20}PyPtSnSe solid was suspended in a solution of 20 mL of FM containing 4 g of C_{12}PyBr. The mixture was aged overnight at 80 °C, filtered, and washed with warm FM and H_2O, and dried under vacuum. The obtained *c*-C_{12}PyPtSnSe product was subsequently used for a reverse ion-exchange experiment with C_{20}PyBr.

Physical Measurements. The characterization procedures and methods involving X-ray diffraction, thermogravimetric analyses (TGA), C, H, and N elemental analysis, UV/vis/near-IR spectroscopy, Mössbauer spectroscopy, scanning and transmission electron microscopy, and energy dispersive analysis have been described in detail elsewhere.[23]

Results and Discussion

The assembly of $[Sn_2Se_6]^{4-}$ anions[25] in FM solution with Pt^{2+} in the presence of octadecyl- or eicosadecylpyridinium molecules acting as the surfactant template (C_nPyBr, $n = 18, 20$) resulted the formation of novel cubic semiconducting mesophases with 100% single-crystal particle morphology. These materials are denoted as *c*-C_nPyPtSnSe ($n = 18, 20$). The elemental composition was determined by energy-dispersive microprobe analysis (SEM/EDS) and elemental C, H, and N and thermogravimetric analysis (TGA); see Table 1. These

(14) (a) Yang, C.-M.; Sheu, H.-S.; Chao, K.-J. *Adv. Funct. Mater.* **2002**, *12*, 143−148. (b) Shin, H. J.; Ryoo, R.; Liu, Z.; Terasaki, O. *J. Am. Chem. Soc.* **2001**, *123*, 1246−1247. (c) Kang, H.; Jun, Y.; Park, J. I.; Lee, K. B.; Cheon, J. *Chem. Mater.* **2000**, *12*, 3530. (d) Huang, M. H.; Choudrey, A.; Yang, P. D. *Chem. Commun.* **2000**, 1063−1064.
(15) (a) Kohn, R.; Froba, M. *Catal. Today* **2001**, *68*, 227−236. (b) Dapurkar, S. E.; Badamali, S. K.; Selvam, P. *Catal. Today* **2001**, *68*, 63−68.
(16) (a) Kaneda, M.; Tsubakiyama, T.; Carlsson, A.; Sakamoto, Y.; Ohsuna, T.; Terasaki, O.; Joo, S. H.; Ryoo, R. *J. Phys. Chem. B* **2002**, *106*, 1256−1266. (b) Joo, S. H.; Choi, S. J.; Oh, I.; Kwak, J.; Liu, Z.; Terasaki, O.; Ryoo, R. *Nature* **2001**, *412*, 169−172.
(17) (a) Rajeshwar, K.; Tacconi, N. R.; Chenthamarakshan, C. R. *Chem. Mater.* **2001**, *13*, 2765−2782. (b) Sohn, L. L. *Nature* **1998**, *394*, 131−132. (c) Murray, C. B.; Kagan, C. R.; Bawendi, M. G. *Science* **1995**, *270*, 1335−1338.
(18) Norris, D. J.; Vlasov, Y. A. *Adv. Mater.* **2001**, *13*, 371−376.
(19) (a) Li, H. L.; Laine, A.; O'Keeffe, M.; Yaghi, O. M. *Science* **1999**, *283*, 1145−1147. (b) Ozin, G. A. *Supramol. Chem.* **1995**, *6*, 125. (c) Li, H. L.; Eddaoudi, M.; Laine, A.; O'Keeffe, M.; Yaghi, O. M. *J. Am. Chem. Soc.* **1999**, *121*, 6096−6097. (d) Beecroft, L. L.; Ober, C. K. *Chem. Mater.* **1997**, *9*, 1302−1317.
(20) (a) Braun, P. V.; Osenar, P.; Tohver, V.; Kennedy, S. B.; Stupp, S. I. *J. Am. Chem. Soc.* **1999**, *121*, 7302−7309. (b) Ozin, G. A. In *Materials Chemistry*; Interrante, L. V., Casper, L. A., Ellis, A., Eds.; American Chemical Society: Washington, DC, 1995; Vol. 245, pp 335−371. (c) Weiss, D.; Richter, K.; Menschig, A.; Bergmann, R.; Schweizer, H.; Vonklitzing, K.; Weimann, G. *Phys. Rev. Lett.* **1993**, *70*, 4118−4121.
(21) Stupp, S. I.; Braun, P. V. *Science* **1997**, *277*, 1242−1248.
(22) Trikalitis, P. N.; Rangan, K. K.; Bakas, T.; Kanatzidis, M. G. *Nature* **2001**, *410*, 671−675.
(23) Trikalitis, P. N.; Rangan, K. K.; Kanatzidis, M. G. *J. Am. Chem. Soc.* **2002**, *124*, 2604−2613.
(24) (a) MacLachlan, M. J.; Coombs, N.; Ozin, G. A. *Nature* **1999**, *397*, 681−684. (b) Rangan, K. K.; Trikalitis, P. N.; Kanatzidis, M. G. *J. Am. Chem. Soc.* **2000**, *122*, 10230−10231. (c) Rangan, K. K.; Trikalitis, P. N.; Bakas, T.; Kanatzidis, M. G. *Chem. Commun.* **2001**, 809−810.
(25) Eisenmann, B.; Hansa, J. *Z. Kristallogr.* **1993**, *203*, 299−300.

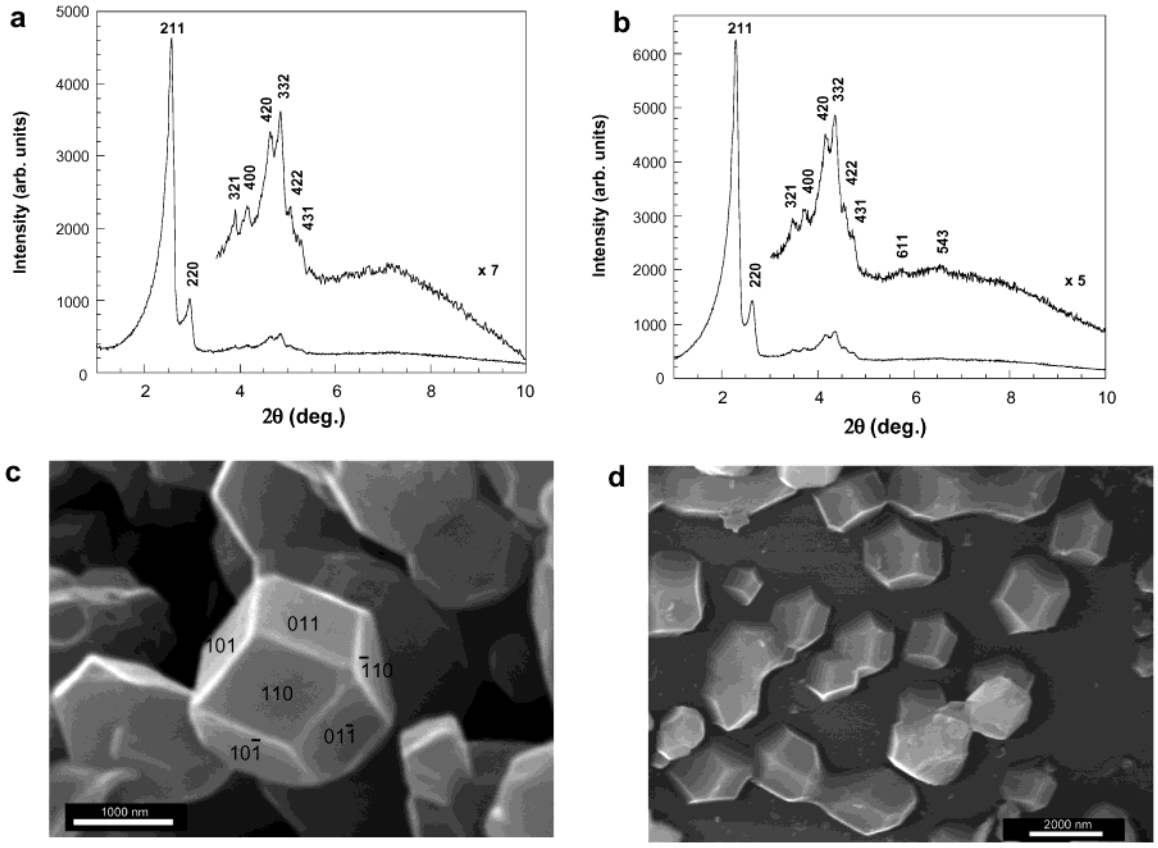

Figure 1. X-ray diffraction patterns of mesostructured platinum chalcogenides: (a) *c*-C_{18}PyPtSnSe; (b) *c*-C_{20}PyPtSnSe (Cu Kα radiation, scan speed 0.1 deg/min). At $2\theta > 10°$ the patterns contain no observable Bragg peaks under the conditions of our experiment. Instead, broad diffuse scattering was observed, much like in all surfactant templated mesostructured materials. (c, d) High-resolution SEM images of *c*-C_{20}PyPtSnSe single crystals with rhombic dodecahedral morphology. The face indices of the crystals are shown in (c). The images were recorded with a JEOL JSM-6400V scanning electron microscope. The samples were gold sputtered to avoid charging effects on the images.

results are consistent with the stoichiometric formula $(C_nPy)_2Pt[Sn_2Se_6]$ ($n = 18$, 20).

The X-ray powder diffraction (XRD) patterns of *c*-C_nPyPtSnSe materials show up to 10 Bragg diffraction peaks in the low-angle $2° < 2\theta < 7°$ region resembling the XRD patterns of high-quality mesostructured cubic MCM-48 silica;[13,26,27] see Figure 1a,b.

The XRD patterns of *c*-C_nPyPtSnSe are fully indexed to a cubic unit cell belonging to the $Ia\bar{3}d$ space group, with refined unit cell parameters of 85.1 ± 0.2 and 95.0 ± 0.1 Å for *c*-C_{18}PyPtSnSe and *c*-C_{20}PyPtSnSe, respectively; see Table 2.

High-resolution scanning electron images (SEM) of *c*-C_nPyPtSnSe materials reveal that the particles are in fact single crystals with rhombic dodecahedral cubosome morhology, as large as 2 μm. Shown in Figure 1c,d are representative SEM images of *c*-C_{20}PyPtSnSe cubosomes. These polyhedral-shaped crystals display smooth *hkl* indexable faces and sharp edges. The product consists entirely of cubosome particles. It is highly uncommon for mesostructured materials to show single-crystal external morphology. For example, in the case of cubic $Ia\bar{3}d$ silica MCM-48, synthesis of single-crystal polyhedral-shaped particles on the micrometer length scale requires extremely narrow experimental conditions.[13,27] The pore system in $Ia\bar{3}d$ symmetry forms an enantiomeric pair of noninterpenetrating channels running along the [100] and [110] directions,[28] while the inorganic wall presumably forms a bicontinuous minimal gyroid surface wrapped around these channels.[29] Therefore, the formation of faceted crystal particle morphology with high external symmetry is a result of the excellent and long-range organization and propagation of the inorganic wall around the

Table 2. Observed Bragg Reflections and Indexing for *c*-C_nPyPtSnSe ($n = 18$, 20) Materials

	d values (Å)	
hkl[a]	*c*-C_{18}PyPtSnSe ($a_c = 85.1 \pm 0.2$ Å)	*c*-C_{20}PyPtSnSe ($a_c = 95.0 \pm 0.1$ Å)
211	34.2	38.6
220	29.8	33.3
321	22.6	25.4
400	21.2	23.7
420	19.0	21.1
332	18.2	20.3
422	17.4	19.4
431	16.8	18.7
611		15.4
543		13.5

[a] Systematic absences consistent with the $Ia\bar{3}d$ space group.

(26) (a) Benjelloun, M.; Van der Voort, P.; Cool, P.; Collart, O.; Vansant, E. F. *Phy. Chem. Chem. Phys.* **2001**, *3*, 127−131. (b) Schumacher, K.; Ravikovitch, P. I.; Du Chesne, A.; Neimark, A. V.; Unger, K. K. *Langmuir* **2000**, *16*, 4648−4654. (c) Kruk, M.; Jaroniec, M.; Ryoo, R.; Kim, J. M. *Chem. Mater.* **1999**, *11*, 2568−2572. (d) Van der Voort, P.; Mathieu, M.; Mees, F.; Vansant, E. F. *J. Phys. Chem. B* **1998**, *102*, 8847−8851.
(27) Kim, J. M.; Kim, S. K.; Ryoo, R. *Chem. Commun.* **1998**, 259−260.
(28) Carlsson, A.; Kaneda, M.; Sakamoto, Y.; Terasaki, O.; Ryoo, R.; Joo, S. H. *J. Electron Microsc.* **1999**, *48*, 795−798.
(29) (a) Anderson, M. W. *Zeolites* **1997**, *19*, 220−227. (b) Alfredsson, V.; Anderson, M. W.; Ohsuna, T.; Terasaki, O.; Jacob, M.; Bojrup, M. *Chem. Mater.* **1997**, *9*, 2066−2070. (c) Alfredsson, V.; Anderson, M. W. *Chem. Mater.* **1996**, *8*, 1141−1146.

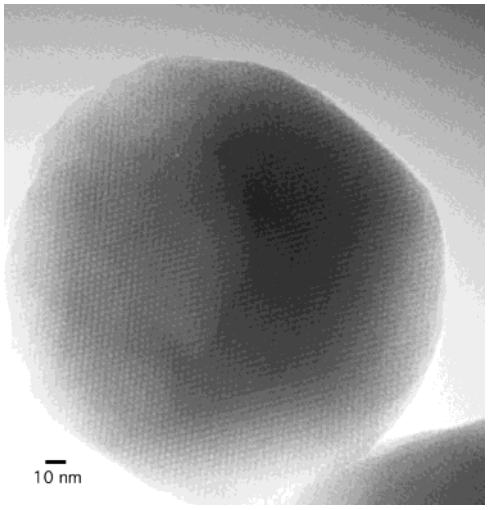

Figure 2. Representative TEM image of a *c*-C_{18}PyPtSnSe single particle viewed down to the [110] cubic plane. High-resolution transmission electron micrographs were obtained with a JEOL 120CX instrument equipped with CeB_6 filament and operating at 120 kV. TEM samples were prepared by gentle grinding the powders and casting on a holey carbon grid.

surfactant-filled mesopores, according to the rule of $Ia\bar{3}d$ symmetry.

The density of *c*-C_{20}PyPtSnSe crystallites was measured, using a standard flotation method with $CH_2Cl_2/BrCH_2CH_2Br$, to be 1.88 g/cm^3. On the basis of the unit cell volume of 857 375 Å^3, the space group symmetry of $Ia\bar{3}d$ ($Z = 48$), and elemental composition, we estimate the chemical formula of the asymmetric unit to be close to "$(C_{20}Py)_{24}Pt_{12}[Sn_2Se_6]_{12}$". This amounts to ~588 non-hydrogen atoms/asymmetric unit. This information will be crucial in future attempts to generate plausible atomic scale models of this structure type. The walls in the silica material MCM-48 are believed to be amorphous at length scales <20 Å, because of the infinitely flexible character of Si−O−Si bond angles. In contrast, the precisely defined nature of the building blocks employed to assemble *c*-C_nPyPtSnSe, their relatively rigid character, and the limited flexibility of M−Se−M′ bond angles make it difficult to make a similar assertion. It is entirely possible that the Pt/Sn/Se framework may in fact be periodic. A crystal with such a large unit cell as *c*-C_{20}PyPtSnSe will generate ~18 000 unique reflections (assuming Cu Kα and $2\theta_{max} \sim 100°$), taking into account the *I*-centered symmetry. However, because the scattering intensity is mostly funneled through the low-angle reflections representing the pore organization, it leaves very little intensity to be distributed over many thousands of reflections. This will result in extremely weak Bragg scattering at wide angles and could explain their absence in the diffraction patterns.

The sharp XRD patterns and single-crystal morphology of the *c*-C_nPyPtSnSe particles betray the excellent mesoscopic order in these materials that is confirmed with direct imaging by transmission electron microscopy (TEM) and selected area electron diffraction experiments (SAED). Figure 2 shows a typical TEM image of a *c*-C_{18}PyPtSnSe single particle viewed down the [110] direction where a remarkably uniform and extensive pore order is clearly visible. Figure 3 shows TEM images and the electron diffraction patterns taken along the [110], [111], and [311] directions, respectively. From the TEM/SAED experiments, the estimated pore−pore separation and unit cell dimensions are in good agreement with those determined by XRD.

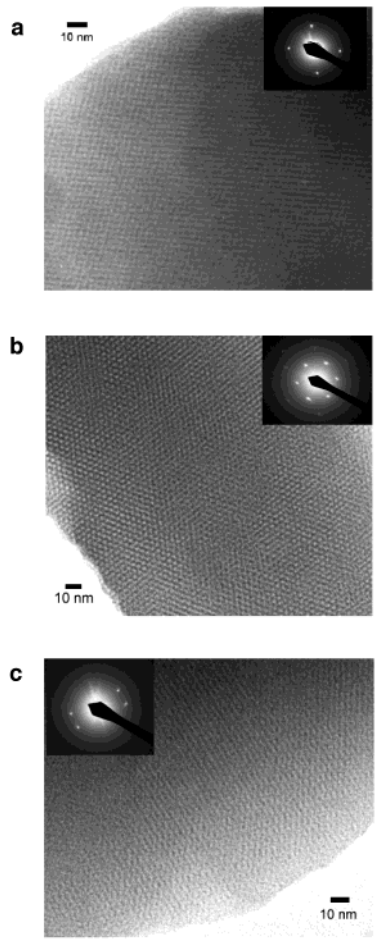

Figure 3. TEM images and corresponding selected area diffraction patterns of *c*-C_{18}PyPtSnSe material viewed down the (a) [110], (b) [111], and (c) [311] crystallographic directions.

^{119}Sn Mössbauer spectroscopy served to identify and characterize the Sn local environment and formal oxidation state in *c*-C_nPyPtSnSe. Figure 4a shows ^{119}Sn Mössbauer spectra for $K_4Sn_2Se_6$ and *c*-C_{18}PyPtSnSe. The corresponding isomer shift, δ, and quadrupole splitting, ΔE_q, parameters for *c*-C_nPyPtSnSe are very similar and characteristic of tetrahedral Sn^{4+} centers.[30]

The pyridinium surfactants C_nPy are not needed to stabilize the cubic structure. Preliminary experiments with long-chain alkyltrimethylammonium halides, C_nTMA ($n = 18$, 20), also gave materials, *c*-C_nTMAPtSnSe, with cubic symmetry and single-crystal morphology although the appearance and X-ray-diffracting quality were poorer. Therefore, we may conclude that the square planar bonding topology of the Pt^{2+} and $[Sn_2Se_6]^{4-}$ building blocks is the key feature responsible for the stabilization of this structure type.

The *c*-C_nPyPtSnSe materials provide the first example of non-oxidic systems that exhibit facile and reversible ion-exchange properties. Remarkably, the surfactant molecules can be ion-exchanged with shorter chain surfactants such as the C_{12}PyBr without loss of the cubic structure and cubosome morphology

(30) Lippens, P. E. *Phys. Rev. B* **1999**, *60*, 4576−4586.

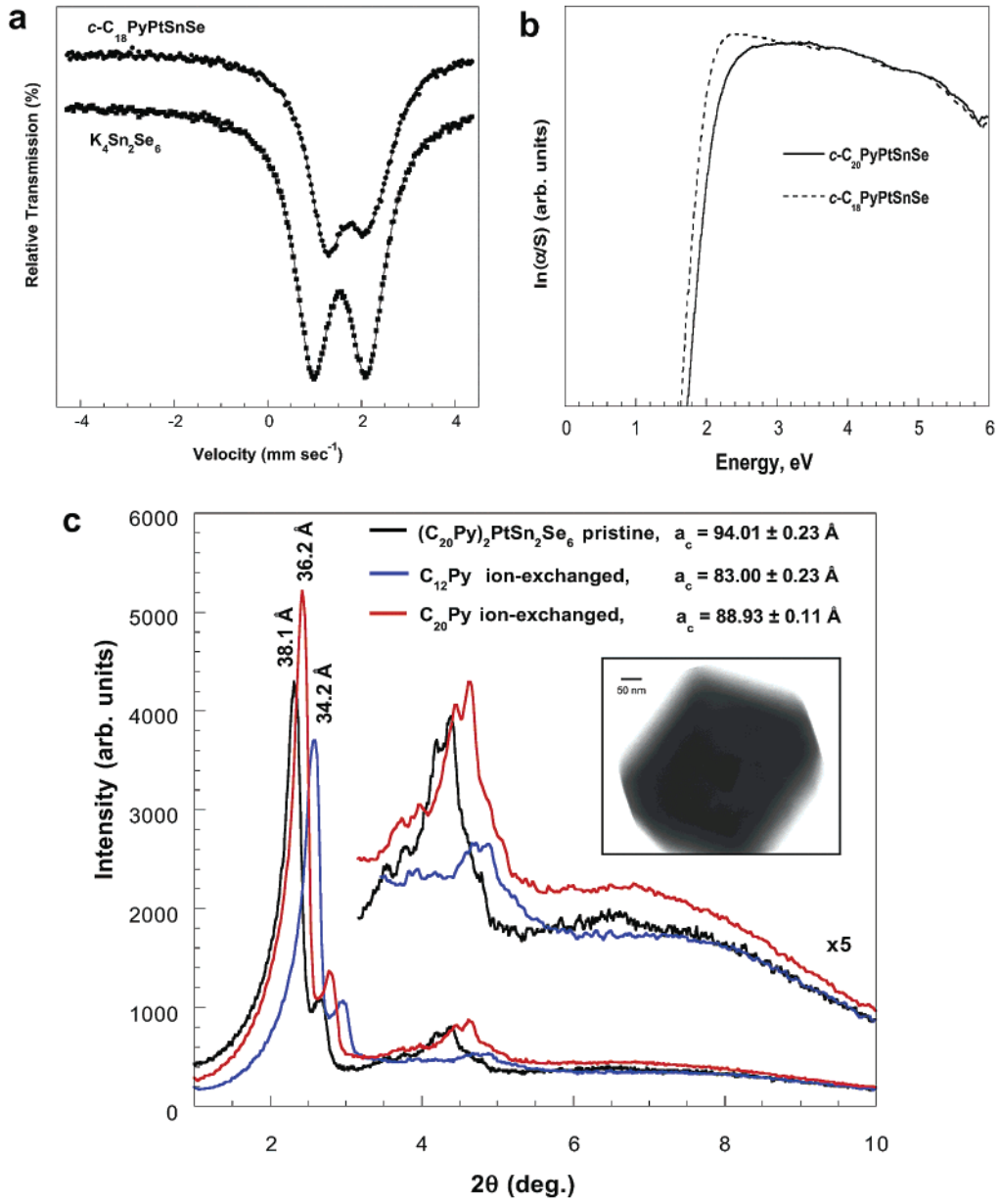

Figure 4. (a) ^{119}Sn Mössbauer spectra (85 K) with derived $\delta/\Delta E_q$ parameters ($K_4Sn_2Se_6$ (standard), 1.53/1.15 mm s^{-1}). The spectrum is consistent with one tetrahedral Sn^{4+} site in an asymmetric environment as expected from the crystal structure of the $[Sn_2Se_6]^{4-}$ anion (*c*-C_{18}PyPtSnSe, 1.62/0.92 (20%) mm s^{-1}, 1.62/0.77 (56%) mm s^{-1}, and 1.89/1.13 (24%) mm s^{-1}). The three slightly different Sn environments suggest the presence of at least three different binding modes for the $[Sn_2Se_6]^{4-}$ units in *c*-C_nPyPtSnSe solids. ^{119}Sn Mössbauer spectra of powder samples were obtained at 85 K in an exchange gas cryostat, using a constant-acceleration spectrometer and a 5 mCi $CaSnO_3$ source kept at room temperature. The isomer shifts are relative to $CaSnO_3$ at room temperature. (b) Solid-state UV−vis absorption spectra of *c*-C_nPyPtSnSe materials. (c) X-ray powder patterns of the pristine *c*-C_{20}PyPtSnSe, $C_{12}Py^+$-exchanged, and $C_{20}Py^+$-exchanged materials. The ion-exchanged products consist entirely of faceted, single-crystal-like particles with cubosome morphology. The inset shows a typical TEM image of a single-crystal-like particle after exchange with $C_{12}Py^+$ ions. The ion-exchanged materials were characterized with elemental analyses and pyrolysis mass spectrometry to confirm the presence of incoming C_nPy molecules in the solid.

(seen by TEM, SEM). Shown in Figure 4c are the X-ray powder patterns of as-synthesized *c*-C_{20}PyPtSnSe along with those from the products after the ion exchange. The C_{12}Py-exchanged material shows up to eight Bragg diffraction peaks, fully indexed to a cubic $Ia\bar{3}d$ unit cell. The C_{12}Py-exhanged solid shows a contraction of the unit cell constant of ∼11 Å relative to the pristine material (Figure 4c). It is important to note here that ion exchange is the only way to prepare *c*-C_{12}PyPtSnSe since the use of C_{12}PyBr surfactant in the initial synthesis afforded material with *hexagonal* pore order and not cubic. Ion exchange was established with full elemental analyses and pyrolysis mass spectrometry of the C_{12}Py-exchanged material which revealed only traces of $C_{20}Py^+$. Interestingly, the C_{12}Py-exchanged solid ion exchanges back with C_{20}PyBr surfactant, to produce the original material which retained the cubic symmetry and cubosome morphology (see XRD pattern in Figure 4c) and unit cell constant of ∼89 Å. The reversible contraction/expansion of the unit cell, with exchange of smaller and larger ions respectively, suggests a robust and elastic framework that can withstand large changes in pore volume.[31] The reasons for the successful ion-exchange properties in these materials are attributed to the three-dimensional cubic structure which renders

the framework accessible from all crystal directions. This is in sharp contrast to the lack of corresponding properties in previously reported hexagonal materials.[23]

The *c*-C_nPyPtSnSe materials are markedly stable over time. Hydrothermally treated samples (at 100 °C over 2 d) showed XRD patterns that were virtually identical to those of freshly prepared samples. The thermal stability was also investigated with thermogravimetric analysis (TGA) and pyrolysis mass spectrometry (MS). The compounds show no appreciable weight loss up to 150 °C. Between 150 and 450 °C weight loss occurs in a two-step process due to surfactant decomposition, and this is evident from the slope change occurring at ~290 °C in the TGA curves. The inorganic residue at 600 °C is an amorphous Pt−Sn−Se phase along with crystalline $SnSe_2$. Pyrolysis mass spectrometry at 250 °C of the released volatiles shows a strong peak with *m*/*z* 79 which corresponds to the pyridyl headgroup of the surfactant, the first species to leave the solid. On further heating $C_nH_{2n+1}Se^+$ were detected showing that the platinum chalcogenide framework is attacked during this process. Although template removal is always a goal to be achieved, it is not necessary to exploit the properties of these systems. On the contrary, organic molecules with interesting electronic or photonic properties anchored to the surfactant could be a way to impart various properties to the structure.[21,32]

c-C_nPyPtSnSe possess the sharpest, well-defined optical absorption edges reported for mesostructured metal chalcogenides; see spectra in Figure 4b. These absorptions, associated with band-gap transitions, are observed at 1.64 and 1.75 eV for *c*-C_{18}PyPtSnSe and *c*-C_{20}PyPtSnSe, respectively, in the same range as those of many important semiconductors such as GaAs (1.43 eV) and CdSe (1.70 eV).

Concluding Remarks

The present results underscore the critical role certain well-selected chalcogenido building blocks can play in the construction of cubic 3D mesostructured semiconductors. The importance of using Pt^{2+} as a linkage metal for the $[Sn_2Se_6]^{4-}$ cluster units (both of square-planar bonding topology) to assemble the cubic structure is revealed, when under the same experimental conditions other transition metals (i.e. Ni^{2+}, Zn^{2+}, Cd^{2+}) failed to produce cubic symmetry. The cubic morphology allows access of the pore space in these materials through ion exchange for the first time. The robustness and flexibility of the inorganic Pt−Sn−Se framework was demonstrated during ion exchange. Up until now chalcogenido mesostructured materials have been available in powder form which permits only powder-averaged studies and makes understanding of their electronic and optical properties more difficult. The ordered single-domain particles of *c*-C_nPyPtSnSe described here point to the highly attractive possibility of creating much larger specimens with no grain boundaries which would be suitable for more sophisticated and detailed property studies that eventually could impact nanotechnological applications. Therefore, a primary goal at this stage is to identify experimental conditions to grow the single-crystal particles to even greater sizes. Finally in the periodic length mesoscales presented by *c*-C_nPyPtSnSe, a strong spatial confinement of charge carriers is anticipated in these nanostructures, because of the generally longer wavelength of electrons or holes. These systems could serve as natural self-assembled antidot arrays that could be used to explore if quantum properties, attributed to antidot behavior, may arise in mesostructured semiconductors.[33]

Acknowledgment. The support of this research by NSF-CRG Grant CHE 0211029 is gratefully acknowledged. This work made use of the SEM and TEM facilities of the Center of Advanced Microscopy at MSU.

JA026367G

(31) We performed ion-exchange experiments using an HCl/EtOH mixture with *c*-C_nTMAPtSnSe, and we were able to extract up to ~50% of the surfactant while maintaining the cubic symmetry and particle morphology. The product shows a contraction of the unit cell parameter by ~25 Å. Elemental analysis using SEM−EDS showed no difference in the Pt:Sn:Se ratio compared with the pristine material. However N_2 absorption measurements showed that the ion-exchanged product has a surface area of <10 m^2/g. This suggests that while the pores in the structure are accessible by outside species via ion exchange, the inorganic framework is able to adjust to the lower organic content by contracting. This elastic property is unique among mesostructured three-dimensional materials and needs to be further investigated.

(32) (a) Scott, B. J.; Wirnsberger, G.; Stucky, G. D. *Chem. Mater.* **2001**, *13*, 3140−3150. (b) Alivisatos, A. P.; Barbara, P. F.; Castleman, A. W.; Chang, J.; Dixon, D. A.; Klein, M. L.; McLendon, G. L.; Miller, J. S.; Ratner, M. A.; Rossky, P. J.; Stupp, S. I.; Thompson, M. E. *Adv. Mater.* **1998**, *10*, 1297−1336.

(33) Schuster, R.; Ensslin, K.; Kotthaus, J. P.; Bohm, G.; Klein, W. *Phys. Rev. B* **1997**, *55*, 2237−2241.